Distinct oligodendrocyte populations have spatial preference and injury-specific responses

Elisa M. Floriddia[1*], Shupei Zhang[1], David van Bruggen[1], João P. Gonçalves dos Santos[1], Müge Altınkök[1], Enric Llorens-Bobadilla[2], Jonas Frisén[2], Gonçalo Castelo-Branco[1,3*]

[1] Laboratory of Molecular Neurobiology, Department Medical Biochemistry and Biophysics, Karolinska Institutet, Biomedicum, 17177 Stockholm, Sweden

[2] Department of Cell and Molecular Biology, Karolinska Institutet, Biomedicum, 17177 Stockholm, Sweden.

[3] Ming Wai Lau Centre for Reparative Medicine, Stockholm node, Karolinska Institutet, 171 77 Stockholm, Sweden

*Co-correspondence: elisa.floriddia@ki.se & goncalo.castelo-branco@ki.se

Abstract

Oligodendrocytes (OLs), the myelinating cells of the central nervous system, are transcriptionally heterogeneous,[1] the origin and functional consequences of which are unknown. Functional heterogeneity of MOLs might correlate with the local environment or their interactions with different neuron types.[2] Here, we show that distinct MOL populations have spatial preference in the mammalian central nervous system and differential susceptibility to traumatic spinal cord injury. We also show that the generation of distinct MOL populations is independent of the OPC developmental origin. We found that OPCs originating from the previously described developmental waves[3-5] have comparable potential to differentiate into the main MOL populations. Furthermore, we found that MOL type 2 (MOL2) is enriched in the spinal cord and almost absent in the brain, while MOL5/6 is enriched with age in all analyzed regions. MOL2 and MOL5/6 also have differential preference for motor and sensory tracts in the spinal cord. In the context of disease, we found that MOL2 and MOL5/6 have differential susceptibility to traumatic spinal cord injury, where MOL2 are lost and MOL5/6 increased their contribution to the OL lineage. Importantly, MOL2 susceptibility is disease specific, as we found MOL2 is not lost in a mouse model of multiple sclerosis. Our results demonstrate that the MOL populations, previously described by single-cell transcriptomics,[1] have distinct spatial preference and responses. We anticipate our study to pave the way for a better understanding of the MOL populations-specific functional roles in development, health, and disease, allowing for better targeting of the OL subtypes important for the regeneration and repair of the central nervous system.

Main text

Oligodendrocytes (OLs) metabolically support axons and increase conduction speed.[6] We have recently reported that the OL lineage is heterogeneous, as it is composed of transcriptionally distinct subpopulations/states during development and disease.[1,7,8] The heterogeneity of the OL lineage does not lie exclusively within the OL transcriptome. Indeed, developmentally distinct oligodendrocyte progenitor cell (OPC) pools generate OL lineage cells with different abilities to respond to demyelination.[9] Mature OLs form myelin internodes of various length and thickness, even along the same axon,[10,11] and show properties regulated at both cell-autonomous and non-autonomous levels.[12,13]

While single-cell RNA-sequencing (scRNAseq) unveiled the transcriptional heterogeneity of the OL lineage and suggested differential enrichment of MOLs in different regions of the CNS,[1] technical limitations, such as differences in viability of cell subpopulations during tissue dissociation,[14] might lead to biased cell enrichments. Thus, we assessed the distribution of the OL

54 lineage within white matter (WM) and grey matter (GM) of the brain and spinal cord *in situ*
55 (Extended Data Fig. 1A-B). We performed immunohistochemistry (IHC) and RNAscope in situ
56 hybridization (ISH) for Sox10 as a pan marker of the OL lineage and analyzed confocal images of
57 the corpus callosum (WM), somatosensory cortex (GM) and spinal cord dorsal horn (GM). We
58 analyzed the images with a custom automated pipeline (CellProfiler, Extended Data Fig. 1C-F).
59 Ptprz1 (receptor-type tyrosine-protein phosphatase zeta 1), a marker of OPCs and committed OPCs
60 (COPs),[1,7] presented a homogeneous distribution across the analyzed regions (Extended Data Fig.
61 1G, I, K, O. Extended Data Table 1, 2). As expected, we observed a decrease from juvenile to
62 adulthood in the OPCs/COPs (*Ptprz1*$^{+}$-*Sox10*$^{+}$) contribution to the OL lineage cells (*Sox10*$^{+}$),
63 especially in the somatosensory cortex (Extended Data Fig. 1G, I, K, O. Extended Data Table 1, 2).
64 Among the six transcriptionally distinct mature oligodendrocyte populations previously described,
65 MOL1, MOL2, and MOL5/6 present the most distinct gene marker modules,[1,7,8] therefore we
66 analyzed their spatial distribution. *Egr2* (*Early Growth Response 2*; also known as *Krox20*) is
67 expressed specifically by MOL1 in the OL lineage[1] and we observed an even distribution of MOL1
68 within the analyzed regions (Extended Data Fig. 1H, J, L, P. Extended Data Table 1, 2). *Klk6*
69 (*Kallikrein Related Peptidase 6*) is a distinct marker for MOL2.[1,7,8,15] Klk6 has been previously
70 associated with demyelinating pathology in experimental autoimmune encephalomyelitis (EAE)
71 and spinal cord injury (SCI).[16,17] Strikingly, we observed that *Klk6*$^{+}$ MOL2 is a population
72 specifically enriched in the spinal cord and almost absent in the brain (Fig. 1A-B, Extended Data
73 Fig. 1M, Q. Extended Data Table 1, 2). In contrast, MOL5/6, expressing *Ptgds* (*Prostaglandin D2*
74 *Synthase*),[1,7,8] showed a dynamic contribution to the OL lineage, increasing along time and
75 following the myelination temporal pattern. Indeed, at juvenile (P20), MOL5/6 are more abundant
76 in the spinal cord, where myelination is visible early on after birth (P5-6), compared to the brain,
77 where myelination is visible around P10-15. In adulthood (P60), MOL5/6 is the main population
78 contributing to the OL lineage in both brain and spinal cord, being most abundant in the corpus
79 callosum (Fig. 1C-D, Extended Data Fig. 1N, R. Extended Data Table 1, 2). Thus, MOL2 and
80 MOL5/6 present distinct distributions and spatial preference across the CNS, contrary to MOL1.
81
82 The OL lineage derives from distinct progenitor domains and developmental stages,[3] which might
83 have a role in the specification of OPCs into the MOL populations and therefore a role in the
84 observed spatial preference. To investigate this possibility, we first isolated the OL lineage from
85 Emx1::Cre-Sox10::GFP-TdTom mice,[1,5,7] and performed scRNAseq on ventrally (eGFP^{+}) and
86 dorsally (TdTom^{+}) derived OL lineage cells. We analyzed the P60 corpus callosum (Fig. 2A) since
87 this region has representation of OLs derived from both the cortical plate (dorsal domain) and the
88 lateral and medial ganglionic eminences (ventral domains of the embryonic forebrain).[5] As

expected,[5] a greater proportion of TdTom$^+$ OL lineage was obtained, (Fig. 2A, D. Extended Data Fig. 2B, Extended Data Table 3). Clustering analysis with GeneFocus[7,18] of 2,853 OL lineage cells led to the identification of the previously identified OL lineage subpopulations (Fig. 2B, Extended Data Fig. 2A-B).[1,19] Importantly, the contribution of ventrally- and dorsally-derived OL lineage cells to each cluster was comparable (Fig. 2C-D), suggesting that the developmental waves have similar potential to generate the transcriptionally distinct OL lineage subpopulations.

Ventrally-derived and dorsally-derived OL lineage cells arise during embryonic and early-postnatal development, respectively.[3,4,20] We thus further performed lineage tracing using the Pdgfrα::CreERT1-loxP-GFP mouse model[21] to fate map the progeny of pre-OPCs appearing at E12.5[7] or OPCs at P3-5 (Fig. 2E). Postnatal recombination of the Pdgfrα::CreER^{T1}-GFP mice results in the assessment of OPCs arising at both postnatal stages and remaining pre-OPCs, while E12.5 recombination allows the assessment of ventral pre-OPCs arising exclusively from this embryonic stage. Our recombination strategy labelled the majority of the lineage in the juvenile CNS (95.43 ± 6.22% of the Sox10$^+$ cells were positive for the eGFP reporter in the cortex, 62.24 ± 2.35% in corpus callosum, and 96.05 ± 1.15% spinal cord, Extended Data Fig. 3A). However, we observed sparser labeling in adulthood (62.38 ± 19.9% of the Sox10$^+$ cells were also positive for the eGFP reporter in the cortex, 44.16 ± 9.04% in the corpus callosum, and 24.32 ± 8.26% in the spinal cord. Extended Data Fig. 3B). This differential labeling suggests a considerable contribution of non-recombined OPCs (GFP$^-$) within the process of life-long continuous addition of new myelinating OLs for myelin homeostasis and in response to experience.[22,23] Importantly, we observed that a subsets of E12.5 pre-OPCs and their progeny do not disappear later in life in any of the analyzed regions (Fig. 2F-H, Extended Data Fig. 3), as previously suggested.[3-5]

We did not observe significant difference in the contribution of the two developmental waves to the MOL1, MOL2, and MOL5/6 populations (Fig. 2H, Extended Data Fig. 3C-Q). While most of the MOL2 in the dorsal spinal cord were derived from E12.5 pre-OPCs at P20, the contribution from postnatally fate mapped OPCs reached comparable levels in adulthood (19.09 ± 4.95% and 23.35 ± 1.28% from the postnatally- and embryonically-derived MOL2, respectively. Extended Data Fig. 3M, O-P). This suggests that postnatally-derived OPCs start differentiating into MOL2 later than embryonically-derived pre-OPCs. In sum, our scRNAseq and lineage tracing data suggest that the domain and time of origin does not influence the OPC specification towards distinct MOL populations. Rather, exposure of OPCs to extrinsic cues during critical windows of migration or differentiation might contribute to MOL diversification at their final localization.

124 Given the preferential localization of MOL2 in the spinal cord (Fig. 1A-B), we further investigated
125 whether MOL2 and MOL5/6 spatial preference relates to functionally distinct regions and tracts in
126 the spinal cord (Fig. 3A). Strikingly, we observed an enrichment of MOL2 in the WM compared to
127 the GM of the spinal cord (Fig. 3B, C. Extended Data Table 4), maintained with age (Fig. 3C.
128 Extended Data Table 4). On the contrary, the MOL5/6 population is enriched in the GM compared
129 to the WM of the spinal cord (Fig. 3F, G. Extended Data Table 4). Interestingly, the MOL2
130 population decreases in the GM of the spinal cord during adulthood (Fig. 3C. Extended Data Table
131 4). In accordance with previous reports,[24-28] in the dorsal white matter, the OL lineage density
132 around the dorsal columns and dorsal corticospinal tract corresponds to the development of
133 myelination (Extended Data Fig. 1F). In the descending dorsal motor corticospinal tract, we
134 observed an increase in the OL lineage with age (Extended Data Fig. 1F. Extended Data Table 4)
135 and constant distribution in the ascending sensory dorsal columns (Extended Data Fig. 1F.
136 Extended Data Table 4). Importantly, we observed they have adjacent distribution for MOL2 and
137 MOL5/6, as when we compared their spatial preference for the GM and WM of the spinal cord
138 (Fig. 3B-C, F-G). Indeed, MOL2 are preferentially found in the dorsal columns (Fig. 3D, E), while
139 MOL5/6 preferentially localize in the dorsal corticospinal tract (Fig. 3H, I. Extended Data Table 4).
140
141 The clear spatial preference of MOL2 and MOL5/6 for different regions and tracts of the spinal
142 cord together with the importance of extrinsic, rather than intrinsic, factors for their diversification
143 suggest that the local environment might have an important role in the physiological properties of
144 MOLs. This might also lead to population specific responses in disease. Traumatic injury of the
145 spinal cord is a chronic pathological condition that leads to loss of locomotor and sensory functions
146 due largely to Wallerian degeneration.[29] We took advantage of two models of traumatic injury:
147 dorsal funiculi transection (an axotomy model of mild severity. Fig. 4A) and severe contusion
148 injury (Fig. 4H). During the remyelination stage following injury, we observed that the OL lineage
149 is still well represented distal to and at the injury site (Fig. 4D-E, K).[30-34] However, in both injury
150 models, we observed a specific loss of MOL2 at the injury site (Fig. 4C-B, F-G,I- J, L), maintained
151 along time (Fig. 4F-G). On the contrary, MOL5/6 reached a higher contribution to the OL lineage at
152 the injury site (Fig. 4C, F-G, J, L) compared to the intact spinal cord (Fig. 3F-I), despite the absence
153 of intact axons. We also assessed the spatial distribution of MOL2 and MOL5/6 in regions of
154 Wallerian degeneration rostral and caudal to the injury site (Fig. 4C, F-G; Extended Data Fig. 4).
155 We observed that the spatial preference of MOL2 and MOL5/6 for the dorsal columns and dorsal
156 corticospinal tract was unaffected by the injury (Extended Data Fig. 3). The contribution of
157 MOL5/6 in the dorsal funiculi rostral and caudal to the injury did not change following injury (18.8
158 ± 2.82% and 18.75 ± 2.9% at 3 and 5 mpi, respectively. Fig. 4F-G and Extended Data Fig. 3), and

159 remained similar to their contribution in the white matter of the intact adult spinal cord (Fig. 3F-G.
160 Extended Data Table 4). Surprisingly, the contribution of MOL2 to the OL lineage in the same
161 regions increased with time (Extended Data Fig. 4B-E). Indeed, 5 mpi, the MOL2 cell density is
162 even greater than found in the WM of the intact adult spinal cord (Fig. 3B-C. Extended Data Table
163 4).
164
165 To assess whether the MOL2 loss is disease specific or a general signature of demyelinating and
166 axonal pathology, we took advantage of experimental autoimmune encephalomyelitis (EAE). EAE
167 is a mouse model of CNS inflammation presenting multifocal lesions characterized by extensive
168 oligodendrocyte loss and Wallerian degeneration. Unlike in the spinal cord injury model, we
169 observed a similar distribution of MOL2 and MOL5/6 in the intact or lesioned white matter of the
170 spinal cord in mice immunized with CFA or MOG_{35-55}, respectively (Fig. 4N-O), consistently with
171 our previous transcriptomic analysis identifying a MOL2 population enriched in the spinal cord of
172 EAE mice.[18] In summary, our data indicates that MOL2 is specifically lost and increase their
173 contribution to the OL lineage in regions of Wallerian degeneration following traumatic spinal cord
174 injury. MOL2 might be associated with circuit remodeling, resulting from sprouting of intact axons
175 proximal to the injury site, while the injury site might present factors stimulating MOL5/6 survival
176 or resident OPCs preferentially differentiation to MOL5/6.[12,35,36] Altogether, our data show OL
177 lineage populations present disease specific susceptibility.
178
179 Here, we unveiled that distinct MOL populations have spatial preference in the mammalian central
180 nervous system and differential susceptibility to traumatic spinal cord injury. Additionally, we show
181 that the generation of distinct MOL populations is independent of the OPC developmental origin,
182 and the MOL population-specific susceptibility to traumatic injury. Our data suggest that MOL5/6
183 might be an OL population associated with adaptive myelination, as MOL5/6 increases in the
184 corpus callosum and CST from juvenile to adulthood. Indeed, the tracts forming both the corpus
185 callosum and the CST maintain plasticity throughout life, essential for acquisition and maintenance
186 of new motor skills with continuous OL turnover, suggesting that myelin needs to be constantly
187 remodeled (adaptive myelination) in those regions.[22,27,28] In contrast, we show that MOL2
188 preferentially locate in the dorsal columns (sensory tracts), suggesting that MOL2 might be
189 associated with more stable neural circuits or production of myelin favoring fast conduction.
190 Indeed, proprioceptive and mechanoreceptive long projecting fast axons are myelinated early in
191 development and reach complete myelination by juvenile,[28,37] correlating with the high and stable
192 enrichment of MOL2 in this region. Additionally, MOL2 are transiently over-produced in the grey
193 matter of the spinal cord, suggesting that MOL2 selection and correct localization might be

194 regulated by intrinsic mechanisms, such as programmed cell death.[38,39] This observation is in line
195 with the lack of developmental OPC specification into distinct mature OL populations. Our
196 observations fit a model where the mechanisms regulating differentiation of the OL lineage are
197 independent on the domain of origin,[3,4,20] differently than it is for neurons.[40,41]
198
199 The proportion of MOL2 decreases after traumatic spinal cord injury but not in EAE. While both
200 pathologies have common features, such as axonal and myelin loss, they also present differences
201 which might contribute to MOL2s differential susceptibility. So-called quiescent oligodendrocytes
202 has been previously described in Wallerian degeneration.[42-44] In accordance, we observed a
203 considerable presence of MOL2 and MOL5/6 in regions where the dorsal columns and corticospinal
204 tracts undergo axonal degeneration. Thus, Wallerian degeneration most likely does not affect the
205 relative contribution of MOL2 and MOL5/6 to the OL lineage.
206
207 Our results show that specific mature OL populations present differential response to traumatic
208 injury. MOL2 and MOL5/6 might have differential contribution to remyelination, axonal support,
209 action potential conduction, and synapse formation inhibition, processes with potential high impact
210 for regenerative medicine. We anticipate our study to pave the way for further understanding of the
211 MOL populations-specific functional roles in development, health, and disease, allowing for better
212 targeting of the OL subtypes important for the regeneration and repair of the central nervous
213 system.
214
215
216 **Acknowledgements**
217 We would like to thank Sarah Foerster, Richa B. Tripathi, William D. Richardson, and Robin J.M.
218 Franklin for the fruitful discussions and sharing the Emx1::Cre-Sox10::Cre-LoxP-GFP-STOP-
219 TdTom line, Rashid Holtinkoski, Eneritz Agirre, Ana Mendanha Falcão, Alessandra Nanni, Johnny
220 Söderlund, Ahmad Moshref, Tony Jimenez-Baristain, the Facility Management and Administration
221 at Biomedicum (Karolinska Institutet, Stockholm) for laboratory management and support. Dr.
222 Göran Månsson and Connla Edwards at the Biomedicum Imaging Core Facility (Karolinska
223 Institutet, Stockholm), Dr. Jaromir Mikes at the Mass Cytometry National Facility (SciLife Lab,
224 Stockholm); Drs. Karolina Wallenborg, Anna Juréus, Marcela Ferella at the Eukariotic Single Cell
225 Genomics facility (SciLife Lab, Stockholm); Katarina Ericsson, Kristoffer Tenebro Berglund,
226 Johanna Hornstrand at the Comparative Medicine Biomedicum facility (Karolinska Institutet,
227 Stockholm) and their respective facility managements, the National Genomics Infrastructure and
228 Uppmax for providing assistance in massive parallel sequencing and computational infrastructure.

229 The bioinformatics computations were performed on resources provided by the Swedish National
230 Infrastructure for Computing at UPPMAX, Uppsala University. Work in G.C.-B.'s research group
231 was supported by Swedish Research Council (grant 2015-03558), European Union (Horizon 2020
232 Research and Innovation Programme/ European Research Council Consolidator Grant EPIScOPE,
233 grant agreement number 681893), Swedish Brain Foundation (FO2017-0075), Ming Wai Lau
234 Centre for Reparative Medicine, Strategic Research Programme in Neuroscience (StratNeuro) and
235 Karolinska Institutet.
236
237 **Author Contributions:** E.M.F. and G.C.-B. conceived the project, designed the study and
238 interpreted results. E.M.F. and S.Z. performed experiments and analyzed data. J.P.G.S., M.A and
239 E.L.B. performed experiments. D.vB. analyzed data. E.M.F., S.Z., D.vB., E.L.B., J.F., and G.C.-B.
240 discussed the results of the study. E.M.F. and G.C.-B. wrote the manuscript with feedback from all
241 co-authors.
242
243 **Materials and Methods**
244 **Animals**
245 All experimental procedures were performed following the guidelines and recommendation of local
246 animal protection legislation and were approved by the local committee for ethical experiments on
247 laboratory animals in Sweden (Stockholms Norra Djurförsöksetiska nämnd).
248 Mouse lines used in this study are Pdgfrα::CreER^{T1}-RCE, Pdgfrα::CreER^{T1}-ROSA26::LoxP-GFP,[21]
249 Sox10::CreER^{T2}-ROSA26::LoxP-GFP,[45,46] available at The Jackson Laboratory, and Emx1::Cre-
250 Sox10::Cre-LoxP-GFP-STOP-TdTom.[5] Mice were used with the Cre allele in hemizygousity and
251 the reporter gene allele in either hemizygousity or homozygousity.
252 Animals were sacrificed at juvenile (P20-21) and adult stages (P60), injuries were performed on
253 adult mice (P60-P150) and sacrificed three- or five-months post-injury, EAE was induced in adult
254 mice (P90) and terminated when the MOG35-55-immunized mice reached a clinical score of 3.0
255 (limp tail and complete paralysis of the hind legs. P100-110). Both sexes were included in the
256 experiments, except for the contusion spinal cord injury paradigm, where only female mice were
257 used. The following light/dark cycle was used: dawn 6:00-7:00, daylight 7:00-18:00, dusk 18:00-
258 19:00, night 19:00-6:00. Mice were housed to a maximum number of 5 per cage in individually
259 ventilated cages with access to food and water ad libitum.
260
261 **Lineage tracing**
262 To fate map the OPCs generated at E13.5 and present at P3-5, Pdgfrα::CreER^{T1}-RCE,
263 Pdgfrα::CreER^{T1}-ROSA26::LoxP-GFP mice were used.[21] Time-mated females were injected i.p.

264 with 1 mg of tamoxifen (Sigma) at pregnancy day E12.5 or 2 mg once daily when pups were P3 to
265 P5 (tamoxifen reaching the pups via the mother's milk). At this low dose (1mg) of tamoxifen during
266 pregnancy (equivalent to 33 mg/kg of body weight) was used to restrict the labeling to the first
267 appearing OPCs. Indeed at this low dose, tamoxifen is metabolized within 24-36 h after injections
268 (therefore E13.5-E14.0. [47,48]). The litters were then sacrificed as juvenile (P20) or young adults
269 (P60) and brains and spinal cords collected for tissue analysis by RNAscope ISH coupled with IHC.
270

271 **Spinal cord injury and post-operative care**

272 *Dorsal funiculi transection*.

273 Mice were kept under anesthesia with a 2% isoflurane/O2 mixture at 1 litre/minute, after two-three
274 minutes induction with 5% isoflurane/O2 mixture at 1 litre/minute. Body temperature was
275 maintained by keeping the mice on a heating pad (37-39°C) during the whole procedure.
276 The injury site was mid-thoracic (T10). The fur was shaved and the area disinfected with Clinical
277 (DAX. twice) and 70% EtOH (once). The skin was incised, the superficial fat displaced, the
278 prominent vessel (between T7 and T8) was identified and used as reference point. Then, the muscle
279 tissue over T9-11 removed to expose the vertebrae. A T10 laminectomy was performed, the dura
280 mater was removed, and the dorsal funiculi transection was performed with a microknife. Dorsal
281 funiculi transection damages dorsal columns, dorsal corticospinal tract, and partially the dorsal
282 horns. After surgery, the mice were injected i.p. with Buprenorphine (Temgesic®) 0.01 mg/kg of
283 body weight and s.c. with 0.5 ml of 0.9% saline solution. The mice were then placed in their home
284 cages and monitored until fully recovered from anaesthesia. During their postoperative care, mice
285 underwent daily checks for general health status, weight loss, mobility, wounds, swelling,
286 infections, or autophagy of the toes. When mice lost weight after surgery, their diet was
287 supplemented with DietGel® Recovery (Clear H_2O). The mice used in this study did not show self-
288 induced wounds or autophagy of the toes or wound infections.

289 *Contusion*

290 Mice were deeply anesthetized with isoflurane and provided with pre-operative analgesia
291 (Buprenorphine, Schering-Plough, 0.1 mg/kg body weight and Carprofen, Pfizer, 5 mg/kg body
292 weight). A laminectomy was performed at the T8-T9 level to expose the dorsal portion of the spinal
293 cord. the vertebral column was then stabilized with clamps (Precision System Instrumentation, PSI)
294 placed on the foramen of T8 and T10. After the administration of local anaesthesia
295 (Xylocaine/Lidocaine, AstraZeneca, 10 mg/ml, 2 drops on the spinal cord surface), a 70 kDyne
296 contusion was delivered medially over T9 using the Infinite Horizon Impactor (IH-0400, PSI)
297 equipped with a 1.3mm tip. The wounds were then sutured and mice placed in a heated cage until
298 they regained consciousness after which they were transferred to their home cage that was equipped

299 with an elevated floor grid. During the first three days of post-operative care, animals received
300 additional hydration (500ul saline injection daily), antibiotic treatment (Sulphadizine/Trimethoprim,
301 Tribrissen vet., MSD, 100mg/kg body weight per day) and analgesia (Buprenorphine, Schering-
302 Plough, 0.1 mg/kg body weight and Carprofen, Pfizer, 5 mg/kg body weight per day). Bladders
303 were expressed three times per day during the first three days and twice per day until they regained
304 bladder control. Their diet was supplemented with a high energy nutritional supplement (DietGel
305 Boost, Clear H2O) during the first week and starting from 1-2 days prior to the surgery. Body
306 weight was monitored daily during the first week and weekly thereafter. Animals that lost more
307 than 15% of their pre-operative body-weight were euthanized and not included in the study.
308
309 **Experimental Autoimmune Encephalomyelitis**
310 For the induction of chronic EAE, animals were injected subcutaneously with an emulsion of
311 MOG35-55 in CFA or vehicle alone (EK-2110 kit, Hooke Laboratories), followed by the i.p.
312 administration of pertussin toxin in PBS (0.2 µg per animal) for two consecutive days (accordingly
313 to manufacture's instructions). Animals were checked daily to assess general health status, weight
314 loss, wounds, swelling, or infections. When mice lost weight after surgery, their diet was
315 supplemented with DietGel® Recovery (Clear H2O). One mouse showed signs of infection at the
316 subcutaneous injection site and was humanly terminated. The mice were also daily score for clinical
317 sign of EAE (accordingly to manufacturer's instructions).
318
319 **Tissue preparation and sectioning**
320 At the end of the experiments for the visualization in tissue of the OL lineage populations, the
321 animals were deeply anesthetized with ketamine (120 mg/kg of body weight) and xylazine (14
322 mg/kg of body weight) and transcardially perfused with 0.1 M PBS followed by 4% PFA in PBS
323 (pH 7.4 for both solutions). Brains and spinal cords were dissected and post-fixed in 4% PFA in
324 PBS (pH 7.4) at 4°C overnight and cryoprotected in 30% sucrose for 48-36 hours.
325 Tissue was embedded in Tissue-Tek® O.C.T. compound (Sakura). Both brains and spinal cords
326 were coronally cryosectioned (20 and 16 µm, respectively) in 1:10 series. Sections were stored at -
327 80°C until further use.
328
329 **Tissue dissociation and single-cell RNAseq**
330 The corpus callosum of P60 Emx1::Cre-Sox10::Cre-LoxP-GFP-STOP-TdTom[5] was microdissected
331 from two mice and the tissue dissociated into a single-cell suspension, as previously described.[1]
332 Briefly, mice were transcardially perfused with ice-cold oxygenated artificial cerebrospinal fluid
333 (22 mM NaCl, 0.63 mM KCl, 0.4 mM NaH_2PO_4 * $2H_2O$, 6.5 mM $NaHCO_3$, 25 mM Saccharose, 5

334 mM Glucose, 0.5 mM $CaCl_2$, 4 mM $MgSO_4$. pH 7.3) and the brains collected. The tissue was
335 sectioned at the vibrotome in ice-cold artificial cerebrospinal fluid and the corpus callosum
336 microdissected. Tissue dissociation was performed with the Adult Brain Dissociation Kit (Miltenyi
337 Biotec) following manufacturer's instructions (red blood cells removal step was not included). After
338 debris removal, the cells were resuspended in ice-cold 1% BSA in artificial cerebrospinal fluid,
339 filtered with 30 µm filter (Sysmex Partec) and FACS sorted with the BD Influx System (USB. BD
340 FACS™) to separate GFP^+ and $TdTom^+$ OL lineage cells.
341 The sorted cells were processed with the Chromium Single Cell A Chip kit v2 and library prep with
342 the Chromium Single Cell 3´Library & Gel Beads kit v2 (10X Genomics) accordingly to
343 manufacturer's instructions. A total of 3,000 cells for each sample was loaded on the Chromium
344 Single Cell A Chip, although a lower number of cells was recovered in singlet and passed the
345 quality control. The scRNAseq dataset is available at GEO (NCBI). GSE128525[1].
346
347 **RNAscope in situ hybridization (ISH) and immunostaining (IHC)**
348 RNAscope ISH was performed using the RNAscope® Multiplex Fluorescent Detection Reagents
349 Kit v2 (ACD Biotechne) on PFA fixed juvenile, adult, and injured brains and spinal cords
350 accordingly to manufacturer's instructions with some modifications. Briefly, after treatment with
351 boiling 1X target retrieval, the sections were incubated with Protease IV for 20 min at RT, followed
352 by washing and the indicated hybridization and amplification steps. Probes used in this study were
353 designed for mouse Sox10-C1 or -C2 (ACD Biotechne, 435931), Ptgds-C1 (ACD Biotechne,
354 492781), Klk6-C3 (ACD Biotechne, 493751), Egr2-C3 (ACD Biotechne, 407871), Ptprz1-C1
355 (ACD Biotechne, 460991).
356 For lineage tracing experiments and the identification of P20 and P60 OL lineage within tissue from
357 the Pdgfrα::CreERT1-RCE::LoxP-GFP mice,[21,49] the RNAscope ISH was coupled with IHC to
358 detect the GFP reporter or endogenous Sox10. Briefly, after hybridization and amplification steps to
359 detect the mRNA of the target gene markers, the sections were blocked in 5% normal donkey serum
360 (NDS), 0.03% Triton X100 in PBS for 1h at RT and incubated with chicken anti-GFP (AbCam, ab
361 13970) or goat anti-Sox10 (Santa Cruz, sc-17342) primary antibodies 1:200 in 2% NDS, 0.03%
362 Triton X100 in PBS, O.N. at RT. The following day, the sections were incubated with goat anti-
363 chicken AlexaFluor 488 conjugated (AbCam, ab150169) or donkey anti-goat AlexaFluor 647
364 conjugated (LifeTech, A21447) secondary antibodies 1:500 in 2% NDS, 0.03% Triton X100 in

[1] The following secure token has been created to allow review of record GSE128525 while it remains in private status: kfizogqqrhwpnwn

365 PBS, 1h at RT and counterstained with DAPI (1:5,000 in PBS) for 2 min. IHC washing steps were
366 performed with 0.05% Tween-20 in PBS.
367
368 **Image acquisition**
369 Fluorescent images were acquired using the LSM800 confocal microscope set up (Zeiss). To obtain
370 an optimal balance between resolution of RNAscope signal and imaged area, tiled images were
371 acquired with a 40X water objective. The z-stack was kept to 2-3 focal planes with 40 µm step to
372 reduce the probability of false positive cells after image maximum projection.
373
374 **Image analysis**
375 Confocal images were processed with FiJi (ImageJ, NIH) to select the regions of interest (ROIs).
376 ROI images were segmented with a customized CellProfiler pipeline. Briefly, the signals from the
377 individual channels (DAPI, markers, GFP) were segmented; OL lineage cells ($Sox10^+$) were
378 identified using the masking option with the DAPI counterstain. Then, the specific OL lineage
379 populations were identified using the relate objects options with the $Sox10^+$ or $Sox10^+$-GFP^+ cells.
380 Overlay images of the identified objects were exported and used to assess the percentage of cell
381 segmentation error. Spreadsheets containing the number of parent cells (DAPI, $Sox10^+$ or $Sox10^+$-
382 GFP^+ cells) and child objects ($Ptgds^+$, $Klk6^+$, $Egr2^+$, $Ptprz1^+$) were exported and used to calculate
383 the percentage of each population. Based on the average gene expression in scRNAseq dataset [1], we
384 used a cut off of 12, 4, 3, and 7 molecules of $Ptgds^+$, $Klk6^+$, $Egr2^+$, $Ptprz1^+$, respectively, per cells to
385 call the analyzed OL lineage populations.
386 We manually assessed the percentage of error for the automated cell segmentation and attribution
387 on 18 representative images (six images per analyzed region). We recorded a segmentation error in
388 the identification of the nuclei of 6.40 ± 1.07% (SFig.1E). We did not observe any substantial error
389 additional to the nuclei segmentation error when we identified the $Sox10^+$-GFP^+ nuclei by the
390 masking option (SFig.1E). Our analysis is a reliable tool for the fast quantification of cells in large
391 image datasets. We calculated the percentage of cells belonging to the oligodendrocyte lineage over
392 the total number of cells ($DAPI^+$ nuclei) and detected the highest and lowest percentage in the
393 corpus callosum and cortex at both P20 (65.87 ± 2.26% and 10.3 ± 0.62%) and P60 (67.95 ± 4.78%
394 and 20.0 ± 5.13%. SFig.1D). This is in line with the previously described distribution of the OL
395 lineage [50] and the relatively myelination levels of the analyzed regions. The image analysis pipeline
396 is available at the following link: https://github.com/Castelo-Branco-lab/Floriddia_et_al_2019.
397
398 **Clustering analysis**

399 Cells were analyzed using the scater package[51]. Cells with less than 100 UMI counts and more than
400 15,000 were not considered for downstream analysis. Pool normalization was then used for
401 normalization the expression matrix,[52] feature selection was performed by calculating the
402 coefficient of variation and using support vector regression to predict variance for a given gene
403 expression level, all genes showing higher variance than expected were used for downstream
404 analysis. The GeneFocus pipeline[18] was used for gene filtering and Spearman correlation was used
405 to build a KNN-graph after which Louvain clustering was applied. Cells that did not include any
406 shared nearest neighbors were discarded from the clustering as outliers. Due to the limited number
407 of cells present in some populations, we performed additional hierarchical clustering and set the
408 threshold to separate the three main populations, oligodendrocyte progenitor cells (OPCs),
409 committed oligodendrocyte progenitor cells (COPs), and mature oligodendrocytes (MOLs). The
410 hierarchical and Louvain clusters were then combined, where the addition of the hierarchical
411 clustering results led to the separation of COP cluster from the broader original Louvain clusters
412 containing both OPCs and COPs. Code used for scRNAseq analysis is available at
413 https://github.com/Castelo-Branco-lab/GeneFocus.
414
415 **Statistics**
416 Statistics on the spatial distribution of the OL lineage populations was performed using 2-way
417 ANOVA. For multiple comparison analysis, the Sidak's correction was applied.
418 Differential gene expression analysis was performed using pairwise Wilcoxon rank sum tests using
419 the stats package in R, on averaged expression per cluster. Significant genes were selected with a
420 FDR adjusted p-value <0.01. The heatmap displays the most top 20 highest enriched genes as
421 measured by z-score.
422
423
424 **Figure legends**
425 **Fig. 1. Specific mature OL populations have spatial preference in the juvenile and adult**
426 **central nervous system.** (**A, C**) Confocal representative images of the distribution of MOL2
427 (Klk6$^+$ OL lineage cells. A), and MOL5/6 (Ptgds$^+$ OL lineage cells. C) in the dorsal horn (grey
428 matter) of the juvenile (P20) and adult (P60) spinal cord. Scale bar = 20 µm. (**B, D**) Quantification
429 of the MOL2 (B), MOL5/6 (D) distribution in the cortex, corpus callosum, and dorsal horn in
430 juvenile (P20) and adulthood (P60). Percentage of the population is calculated on the total number
431 of OL lineage cells (Sox10$^+$ cells) in the analyzed region. Data are presented as Mean ± SEM. n =
432 6-9 animals per condition. Asterisks indicate a significant difference between conditions (*$p \leq 0.05$,

433 ****p ≤ 0.0001, 2-way ANOVA with Sidak's correction). Cx = cortex, CC = corpus callosum, SC
434 = spinal cord.
435
436 **Fig. 2. The developmental origin does not specify OPCs into distinct MOL subpopulations.**
437 (**A**) Confocal representative images of the P60 brain from Emx1::Cre-SOX10::GFP-TdTom mouse.
438 Dashed outline highlights the corpus callosum and dissected region used for scRNAseq. (**B-C**) t-
439 Distributed stochastic neighbor embedding (t-SNE) plots showing the OL lineage composition
440 determined by hierarchical clustering (B) and the $TdTom^+$ and GFP^+ OL lineage cells contribution
441 to the clusters (C). (**D**) Frequency distribution of the $TdTom^+$ and GFP^+ OL lineage cells forming
442 the major clusters. (**E**) Schematic overview of the fate mapping experimental design. Green arrows
443 shows the GFP expression timeline 24h delayed from the time of tamoxifen injection. (**F-G**)
444 Confocal representative images show the MOL5/6 ($Ptgds^+$-GFP^+ OL lineage cells differentiated
445 from pre- (TM E12.5) or postnatal (TM P3-5) OPCs. Scale bar = 20 µm. Sox10 was detected by
446 RNAscope ISH in F and by IHC in G. (**H**) Percentages of the fate mapped OPCs-COPs ($Ptprz1^+$-
447 GFP^+ OL lineage cells), MOL1 ($Egr2^+$-GFP^+ OL lineage cells), MOL2 ($Klk6^+$-GFP^+ OL lineage
448 cells), and MOL5/6 ($Ptgds^+$-GFP^+ OL lineage cells) populations are calculated on the total number
449 of fate mapped OL lineage cells ($Sox10^+$-GFP^+ cells) in the juvenile and adult corpus callosum.
450 Data are presented as Mean ± SEM. n = 3-5 animals per condition. Asterisks indicate a significant
451 difference between conditions (**p ≤ 0.01, ***p ≤ 0.0001, 2-way ANOVA with Sidak's
452 correction). TM = tamoxifen, OPC = oligodendrocyte progenitor cell, COP = committed OPC,
453 NFOL = newly formed oligodendrocyte, MFOL = myelin forming oligodendrocyte, MOL = mature
454 oligodendrocyte, TdTom = tandem duplicated tomato, GFP = green fluorescent protein.
455
456 **Fig. 3. MOL2 and MOL5/6 are specifically enriched in adjacent regions of the juvenile and**
457 **adult spinal cord.** (**A**) Schematics of a coronal section of the spinal cord. Highlighted in blue and
458 red the white matter regions where the axons forming the dorsal columns and dorsal corticospinal
459 tract run, respectively. (**B, D**) Confocal representative images show the enrichment of MOL2
460 ($Klk6^+$ OL lineage cells) in the white matter of the spinal cord (B) and at the level of the dorsal
461 columns (D). (**F, H**) Confocal representative images show the enrichment of MOL5/6 ($Ptgds^+$ OL
462 lineage cells) in the grey matter of the spinal cord (F) and at the level of the dorsal corticospinal
463 tract (H). Scale bar = 100 µm. (**C, E, G, I**) Quantification of the MOL2 and MOL5/6 distribution in
464 the white and grey matter of the spinal cord (C, G) and at the level of the dorsal corticospinal tract
465 and dorsal columns (E, I) in juvenile (P20) and adulthood (P60). Percentage of the population is
466 calculated on the total number of OL lineage cells ($Sox10^+$ cells) in the analyzed region. Data are
467 presented as Mean ± SEM. n = 3-9 animals per condition. Asterisks indicate a significant difference

468 between conditions (*p ≤ 0.05, **p ≤ 0.01, ***p ≤ 0.001, 2-way ANOVA with Sidak's correction).
469 GM = grey matter, WM = white matter, DC = dorsal columns, dCST = dorsal corticospinal tract.
470
471 **Fig. 4. MOL2 and MOL5/6 show differential and disease-specific susceptibility.** (**A-B, H-I, M**)
472 Schematic of the analysis lesion model (A, H, M), level of the lesions (T10. B-I) and distance of the
473 rostral and caudal analyzed segments (B-I). (**C, J, N**) Confocal representative images of the lesions
474 following dorsal funiculi transection (C) and contusion (J) injuries, as well as in EAE (N), showing
475 the specific loss of MOL2 (Klk6$^+$ OL lineage cells) and the high repopulation by MOL5/6 (Ptgds$^+$
476 OL lineage cells) of the lesions following traumatic injury of the spinal cord. Yellow dashed lines
477 highlight the lesion sites. White rectangles highlight the regions shown in higher magnification.
478 Scale bar = 100 µm. (**D-G, K-L, O**) Quantification of the OL lineage (D-E, K) and the MOL
479 subpopulations away and at the traumatic injury sites (F-G, L) and in EAE lesions (O). Percentage
480 of the MOL2 and MOL5/6 subpopulations was calculated on the total number of OL lineage cells
481 (Sox10$^+$ cells). Dashed grey line marks the average percentage of the OL lineage cells in the intact
482 adult spinal cord (D-E, K). Data are presented as Mean ± SEM. n = 4-7 animals per condition.
483 Asterisks indicate a significant difference between conditions (*p ≤ 0.05, **p ≤ 0.01, 2-way
484 ANOVA with Sidak's correction). SCI = spinal cord injury, mpi = months post-injury, T10 =
485 thoracic vertebra 10, CFA = Complete Freund´s Adjuvant, MOG35-55 = Myelin Oligodendrocyte
486 Glycoprotein, peptide fragment 35-55, PTX = Pertussin Toxin.
487
488 **Extended Data Fig. 1. Spatial distribution of OL populations in the juvenile and adult central**
489 **nervous system.** (**A-B**) Schematics of coronal sections of the mouse brain (A) and spinal cord (B).
490 Red squares highlight the systematically analyzed CNS regions. (**C**) Schematic overview and
491 representative analyzed image output of the customized CellProfiler pipeline used in this study. (**D,**
492 **F**) Percentage of the OL lineage cells (Sox10$^+$ cells) calculated on the total number of nuclei shows
493 the expected differential enrichment of the OL lineage in the analyzed regions. Data are presented
494 as Mean ± SEM. n = 5-8 animals per condition. (**E**) Percentage of the segmentation error of the
495 used pipeline. Data are presented as Mean ± SEM. n = 5-18 images per condition. (**G-H, K-R**)
496 Confocal representative images of the distribution of OPC-COPs (Ptprz1$^+$ OL lineage cells. G, K,
497 O), MOL1 (Egr2$^+$ OL lineage cells. H, L, P), MOL2 (Klk6$^+$ OL lineage cells. M, Q), and MOL5/6
498 (Ptgds$^+$ OL lineage cells. N, R) in the dorsal horn (grey matter) of the juvenile (P20) and adult
499 (P60) spinal cord (G-H), cortex (K-N), and corpus callosum (O-R). Scale bar = 20 µm. (**I-J**)
500 Quantification of the OPCs-COPs (I), MOL1 (J) distribution in the cortex, corpus callosum, and
501 dorsal horn in juvenile (P20) and adulthood (P60). Percentage of the population is calculated on the
502 total number of OL lineage cells (Sox10$^+$ cells) in the analyzed region. Data are presented as Mean

503 ± SEM. n = 6-9 animals per condition. Asterisks indicate a significant difference between
504 conditions (*$p \leq 0.05$, **$p \leq 0.01$, ***$p \leq 0.001$, ****$p \leq 0.0001$, 2-way ANOVA with Sidak's
505 correction). Cx = cortex, CC = corpus callosum, SC = spinal cord, DC = dorsal columns, dCST =
506 dorsal corticospinal tract.
507
508 **Extended Data Fig. 2. Louvain clustering analysis of the OL lineage cells.** (**A**) Violin plots
509 depicting the expression of canonical markers for OPCs, MOL1, MOL2 and MOL5/6; (**B**) Heat-
510 map of differential gene expression highlighting the enriched gene modules (right) characterizing
511 the identified clusters (below) by Louvain clustering analysis. Distance matrix = Spearmann
512 correlation.
513
514 **Extended Data Fig. 3. Pre- and postnatal OPCs equally contribute to the generation of MOL**
515 **populations in the juvenile and adult central nervous system.** (**A-B**) Percentage of the fate
516 mapped OL lineage cells ($Sox10^+$-GFP^+ cells) derived by OPCs labeled at E12.5 and P3-5
517 calculated on the total number of OL lineage cells ($Sox10^+$ cells) at juvenile (A) and adulthood (B).
518 (**C-F, H-N**) Confocal representative images show embryonically (TM E12.5)- and postnatally (TM
519 P3-5)-derived OPCs-COPs ($Ptprz1^+$-GFP^+ OL lineage cells. C, H, K), MOL5/6 ($Ptgds^+$-GFP^+ OL
520 lineage cells. D, L), MOL2 ($Klk6^+$-GFP^+ OL lineage cells. E, I, M), MOL1 ($Egr2^+$-GFP^+ OL
521 lineage cells. F, J, N) in the adult (P60) cortex (C-F), corpus callosum (H-J), and dorsal horn of the
522 spinal cord (K-N). Scale bar = 20 μm. (**G, O**) Percentages of the fate mapped OPCs-COPs ($Ptprz1^+$-
523 GFP^+ OL lineage cells), MOL1 ($Egr2^+$-GFP^+ OL lineage cells), MOL2 ($Klk6^+$-GFP^+ OL lineage
524 cells), and MOL5/6 ($Ptgds^+$-GFP^+ OL lineage cells) populations are calculated on the total number
525 of fate mapped OL lineage cells ($Sox10^+$-GFP^+ cells) in the juvenile and adult cortex (G) and spinal
526 cord (O). (**P-Q**) Percentages of the embryonically (TM E12.5)- and postnatally (TM P3-5)-derived
527 MOL2 ($Klk6^+$-GFP^+ OL lineage cells. P), and MOL5/6 ($Ptgds^+$-GFP^+ OL lineage cells. (Q)
528 populations are calculated on the total number of fate mapped OL lineage cells ($Sox10^+$ -GFP^+
529 cells) in the spinal cord white and grey matter. Data are presented as Mean ± SEM. n = 3-5 animals
530 per condition. Asterisks indicate a significant difference between conditions (*$p \leq 0.05$, **$p \leq 0.01$,
531 ***$p \leq 0.001$, ***$p \leq 0.0001$, 2-way ANOVA with Sidak's correction). TM = tamoxifen, GFP =
532 green fluorescent protein, GM = grey matter, WM = white matter.
533
534 **Extended Data Fig. 4. MOL2 population expands away form the injury site but maintain its**
535 **spatial preference following spinal cord injury.** (**A**) Confocal representative images of the dorsal
536 spinal cord region 10-5 mm rostral to the injury site showing the maintained MOL2 ($Klk6^+$ OL
537 lineage cells) and MOL5/6 ($Ptgds^+$ OL lineage cells) spatial preference 5 months post-injury. White

538 dashed lines highlight the dorsal funiculi. Scale bar = 100 μm. (**B-E**) Percentages of the MOL2
539 (Klk6$^+$ OL lineage cells) and MOL5/6 (Ptgds$^+$ OL lineage cells) populations are calculated on the
540 total number of OL lineage cells (Sox10$^+$ cells) in the dorsal columns (B-C) and dorsal corticospinal
541 tract (D-E) 5-10mm rostral and caudal to the injury site. Data are presented as Mean ± SEM. n = 5-
542 7 animals per condition. Asterisks indicate a significant difference between conditions (*p ≤ 0.05,
543 **p ≤ 0.01, ***p≤ 0.001, 2-way ANOVA with Sidak's correction). mpi = months post-injury.
544
545 **Extended Data Table 1. Quantification of the OL subpopulations contribution to the OL**
546 **lineage.** Percentage of the OPC-COPs (Ptprz1$^+$ OL lineage cells), MOL1 (Egr2$^+$ OL lineage cells),
547 MOL2 (Klk6$^+$ OL lineage cells), and MOL5/6 (Ptgds$^+$ OL lineage cells) contribution to the OL
548 lineage (Sox10$^+$ cells) in the regions of interest in juvenile (P20) and adulthood (P60). We imaged
549 0.3, 0.13, and 0.4 mm2 of the sensorimotor cortex, corpus callosum, and dorsal spinal cord per
550 tissue section, respectively. Minimum three sections per animal were analyzed. Data are presented
551 as Mean ± SEM. n = 4-9 animals per condition.
552
553 **Extended Data Table 2. Average number of the quantified cells per analyzed section.** Average
554 number of the OL lineage cells (Sox10$^+$) and OPC-COPs (Ptprz1$^+$ OL lineage cells), MOL1 (Egr2$^+$
555 OL lineage cells), MOL2 (Klk6$^+$ OL lineage cells), and MOL5/6 (Ptgds$^+$ OL lineage cells) counted
556 per region of interest in juvenile (P20) and adulthood (P60) per section. We imaged 0.3, 0.13, and
557 0.4 mm2 of the sensorimotor cortex, corpus callosum, and dorsal spinal cord per tissue section,
558 respectively. Mimimum three sections per animal were analyzed. Data are presented as Mean ±
559 SEM. n = 4-9 animals per condition.
560
561 **Extended Data Table 3. Counting of analyzed cells by scRNAseq.**
562
563 **Extended Data Table 4. Quantification of the OL subpopulations contribution to the OL**
564 **lineage.** Percentage of the MOL2 (Klk6$^+$ OL lineage cells) and MOL5/6 (Ptgds$^+$ OL lineage cells)
565 contribution to the OL lineage (Sox10$^+$ cells) in the spinal cord regions in juvenile (P20) and
566 adulthood (P60). Minimum three sections per animal were analyzed. Data are presented as Mean ±
567 SEM. n = 5-7 animals per condition.
568
569 **References**

570 1 Marques, S. *et al*. Oligodendrocyte heterogeneity in the mouse juvenile and adult central
571 nervous system. *Science* **352**, 1326-1329, doi:10.1126/science.aaf6463 (2016).
572 2 Zonouzi, M. *et al*. Individual Oligodendrocytes Show Bias for Inhibitory Axons in the
573 Neocortex. *Cell Rep* **27**, 2799-2808 e2793, doi:10.1016/j.celrep.2019.05.018 (2019).

3 Richardson, W. D., Kessaris, N. & Pringle, N. Oligodendrocyte wars. *Nat Rev Neurosci* **7**, 11-18, doi:10.1038/nrn1826 (2006).
4 Kessaris, N. *et al*. Competing waves of oligodendrocytes in the forebrain and postnatal elimination of an embryonic lineage. *Nat Neurosci* **9**, 173-179, doi:10.1038/nn1620 (2006).
5 Tripathi, R. B. *et al*. Dorsally and ventrally derived oligodendrocytes have similar electrical properties but myelinate preferred tracts. *J Neurosci* **31**, 6809-6819, doi:10.1523/JNEUROSCI.6474-10.2011 (2011).
6 Simons, M. & Nave, K. A. Oligodendrocytes: Myelination and Axonal Support. *Cold Spring Harbor perspectives in biology* **8**, a020479, doi:10.1101/cshperspect.a020479 (2015).
7 Marques, S. *et al*. Transcriptional Convergence of Oligodendrocyte Lineage Progenitors during Development. *Dev Cell* **46**, 504-517 e507, doi:10.1016/j.devcel.2018.07.005 (2018).
8 Falcão, A. M. *et al*. Disease-specific oligodendrocyte lineage cells arise in multiple sclerosis. *Nature Medicine*, doi:10.1038/s41591-018-0236-y (2018).
9 Crawford, A. H., Tripathi, R. B., Richardson, W. D. & Franklin, R. J. Developmental Origin of Oligodendrocyte Lineage Cells Determines Response to Demyelination and Susceptibility to Age-Associated Functional Decline. *Cell Rep*, doi:10.1016/j.celrep.2016.03.069 (2016).
10 Tomassy, G. S. *et al*. Distinct profiles of myelin distribution along single axons of pyramidal neurons in the neocortex. *Science* **344**, 319-324, doi:10.1126/science.1249766 (2014).
11 Micheva, K. D. *et al*. A large fraction of neocortical myelin ensheathes axons of local inhibitory neurons. *Elife* **5**, doi:10.7554/eLife.15784 (2016).
12 Tomassy, G. S., Dershowitz, L. B. & Arlotta, P. Diversity Matters: A Revised Guide to Myelination. *Trends Cell Biol* **26**, 135-147, doi:10.1016/j.tcb.2015.09.002 (2016).
13 Bechler, M. E., Byrne, L. & Ffrench-Constant, C. CNS Myelin Sheath Lengths Are an Intrinsic Property of Oligodendrocytes. *Curr Biol* **25**, 2411-2416, doi:10.1016/j.cub.2015.07.056 (2015).
14 van den Brink, S. C. *et al*. Single-cell sequencing reveals dissociation-induced gene expression in tissue subpopulations. *Nat Methods* **14**, 935-936, doi:10.1038/nmeth.4437 (2017).
15 Zeisel, A. *et al*. Molecular Architecture of the Mouse Nervous System. *Cell* **174**, 999-1014 e1022, doi:10.1016/j.cell.2018.06.021 (2018).
16 Murakami, K. *et al*. In vivo analysis of kallikrein-related peptidase 6 (KLK6) function in oligodendrocyte development and the expression of myelin proteins. *Neuroscience* **236**, 1-11, doi:10.1016/j.neuroscience.2012.12.073 (2013).
17 Bando, Y. *et al*. Kallikrein 6 secreted by oligodendrocytes regulates the progression of experimental autoimmune encephalomyelitis. *Glia* **66**, 359-378, doi:10.1002/glia.23249 (2018).
18 Falcao, A. M. *et al*. Disease-specific oligodendrocyte lineage cells arise in multiple sclerosis. *Nat Med* **24**, 1837-1844, doi:10.1038/s41591-018-0236-y (2018).
19 Zeisel, A. *et al*. Brain structure. Cell types in the mouse cortex and hippocampus revealed by single-cell RNA-seq. *Science* **347**, 1138-1142, doi:10.1126/science.aaa1934 (2015).
20 Fogarty, M., Richardson, W. D. & Kessaris, N. A subset of oligodendrocytes generated from radial glia in the dorsal spinal cord. *Development* **132**, 1951-1959, doi:10.1242/dev.01777 (2005).
21 Kang, S. H., Fukaya, M., Yang, J. K., Rothstein, J. D. & Bergles, D. E. NG2+ CNS glial progenitors remain committed to the oligodendrocyte lineage in postnatal life and following neurodegeneration. *Neuron* **68**, 668-681, doi:10.1016/j.neuron.2010.09.009 (2010).
22 Tripathi, R. B. *et al*. Remarkable Stability of Myelinating Oligodendrocytes in Mice. *Cell Rep* **21**, 316-323, doi:10.1016/j.celrep.2017.09.050 (2017).
23 Hughes, E. G., Orthmann-Murphy, J. L., Langseth, A. J. & Bergles, D. E. Myelin remodeling through experience-dependent oligodendrogenesis in the adult somatosensory cortex. *Nat Neurosci* **21**, 696-706, doi:10.1038/s41593-018-0121-5 (2018).
24 Joosten, E. A., Gribnau, A. A. & Dederen, P. J. Postnatal development of the corticospinal tract in the rat. An ultrastructural anterograde HRP study. *Anat Embryol (Berl)* **179**, 449-456 (1989).

625 25 Luo, W., Enomoto, H., Rice, F. L., Milbrandt, J. & Ginty, D. D. Molecular identification of
626 rapidly adapting mechanoreceptors and their developmental dependence on ret signaling. *Neuron*
627 **64**, 841-856, doi:10.1016/j.neuron.2009.11.003 (2009).
628 26 Martin, J. H. The corticospinal system: from development to motor control. *Neuroscientist*
629 **11**, 161-173, doi:10.1177/1073858404270843 (2005).
630 27 McKenzie, I. A. *et al*. Motor skill learning requires active central myelination. *Science* **346**,
631 318-322, doi:10.1126/science.1254960 (2014).
632 28 Wolpaw, J. R. Spinal cord plasticity in acquisition and maintenance of motor skills. *Acta*
633 *Physiol (Oxf)* **189**, 155-169, doi:10.1111/j.1748-1716.2006.01656.x (2007).
634 29 Ahuja, C. S. *et al*. Traumatic spinal cord injury. *Nat Rev Dis Primers* **3**, 17018,
635 doi:10.1038/nrdp.2017.18 (2017).
636 30 Emery, E. *et al*. Apoptosis after traumatic human spinal cord injury. *J Neurosurg* **89**, 911-
637 920, doi:10.3171/jns.1998.89.6.0911 (1998).
638 31 Almad, A., Sahinkaya, F. R. & McTigue, D. M. Oligodendrocyte fate after spinal cord
639 injury. *Neurotherapeutics* **8**, 262-273, doi:10.1007/s13311-011-0033-5 (2011).
640 32 Casha, S., Yu, W. R. & Fehlings, M. G. Oligodendroglial apoptosis occurs along
641 degenerating axons and is associated with FAS and p75 expression following spinal cord injury in
642 the rat. *Neuroscience* **103**, 203-218 (2001).
643 33 Li, G. L., Farooque, M., Holtz, A. & Olsson, Y. Apoptosis of oligodendrocytes occurs for
644 long distances away from the primary injury after compression trauma to rat spinal cord. *Acta*
645 *Neuropathol* **98**, 473-480 (1999).
646 34 Lytle, J. M. & Wrathall, J. R. Glial cell loss, proliferation and replacement in the contused
647 murine spinal cord. *Eur J Neurosci* **25**, 1711-1724, doi:10.1111/j.1460-9568.2007.05390.x (2007).
648 35 Leslie, J. R. *et al*. Ectopic myelinating oligodendrocytes in the dorsal spinal cord as a
649 consequence of altered semaphorin 6D signaling inhibit synapse formation. *Development* **138**,
650 4085-4095, doi:10.1242/dev.066076 (2011).
651 36 Kapfhammer, J. P. & Schwab, M. E. Inverse patterns of myelination and GAP-43
652 expression in the adult CNS: neurite growth inhibitors as regulators of neuronal plasticity? *J Comp*
653 *Neurol* **340**, 194-206, doi:10.1002/cne.903400206 (1994).
654 37 Fox, M. W., Inman, O. R. & Himwich, W. A. The postnatal development of the spinal cord
655 of the dog. *J Comp Neurol* **130**, 233-240, doi:10.1002/cne.901300305 (1967).
656 38 Barres, B. A. *et al*. Cell death and control of cell survival in the oligodendrocyte lineage.
657 *Cell* **70**, 31-46 (1992).
658 39 Sun, L. O. *et al*. Spatiotemporal Control of CNS Myelination by Oligodendrocyte
659 Programmed Cell Death through the TFEB-PUMA Axis. *Cell* **175**, 1811-1826 e1821,
660 doi:10.1016/j.cell.2018.10.044 (2018).
661 40 Briscoe, J., Pierani, A., Jessell, T. M. & Ericson, J. A homeodomain protein code specifies
662 progenitor cell identity and neuronal fate in the ventral neural tube. *Cell* **101**, 435-445 (2000).
663 41 Schuurmans, C. & Guillemot, F. Molecular mechanisms underlying cell fate specification in
664 the developing telencephalon. *Current opinion in neurobiology* **12**, 26-34 (2002).
665 42 Brosius Lutz, A. & Barres, B. A. Contrasting the glial response to axon injury in the central
666 and peripheral nervous systems. *Dev Cell* **28**, 7-17, doi:10.1016/j.devcel.2013.12.002 (2014).
667 43 Ludwin, S. K. Oligodendrocyte survival in Wallerian degeneration. *Acta Neuropathol* **80**,
668 184-191 (1990).
669 44 Ludwin, S. K. Oligodendrocytes from optic nerves subjected to long term Wallerian
670 degeneration retain the capacity to myelinate. *Acta Neuropathol* **84**, 530-537 (1992).
671 45 Laranjeira, C. *et al*. Glial cells in the mouse enteric nervous system can undergo
672 neurogenesis in response to injury. *J Clin Invest* **121**, 3412-3424, doi:10.1172/JCI58200 (2011).
673 46 Mao, X., Fujiwara, Y., Chapdelaine, A., Yang, H. & Orkin, S. H. Activation of EGFP
674 expression by Cre-mediated excision in a new ROSA26 reporter mouse strain. *Blood* **97**, 324-326
675 (2001).

676 47 Nakamura, E., Nguyen, M. T. & Mackem, S. Kinetics of tamoxifen-regulated Cre activity in
677 mice using a cartilage-specific CreER(T) to assay temporal activity windows along the
678 proximodistal limb skeleton. *Dev Dyn* **235**, 2603-2612, doi:10.1002/dvdy.20892 (2006).
679 48 Valny, M., Honsa, P., Kirdajova, D., Kamenik, Z. & Anderova, M. Tamoxifen in the Mouse
680 Brain: Implications for Fate-Mapping Studies Using the Tamoxifen-Inducible Cre-loxP System.
681 *Front Cell Neurosci* **10**, 243, doi:10.3389/fncel.2016.00243 (2016).
682 49 Butt, S. J. *et al*. The requirement of Nkx2-1 in the temporal specification of cortical
683 interneuron subtypes. *Neuron* **59**, 722-732, doi:10.1016/j.neuron.2008.07.031 (2008).
684 50 von Bartheld, C. S., Bahney, J. & Herculano-Houzel, S. The search for true numbers of
685 neurons and glial cells in the human brain: A review of 150 years of cell counting. *Journal of*
686 *Comparative Neurology* **524**, 3865-3895, doi:10.1002/cne.24040 (2016).
687 51 McCarthy, D. J., Campbell, K. R., Lun, A. T. & Wills, Q. F. Scater: pre-processing, quality
688 control, normalization and visualization of single-cell RNA-seq data in R. *Bioinformatics* **33**, 1179-
689 1186, doi:10.1093/bioinformatics/btw777 (2017).
690 52 Lun, A. T., Bach, K. & Marioni, J. C. Pooling across cells to normalize single-cell RNA
691 sequencing data with many zero counts. *Genome Biol* **17**, 75, doi:10.1186/s13059-016-0947-7
692 (2016).
693

Floriddia et al., Fig.1

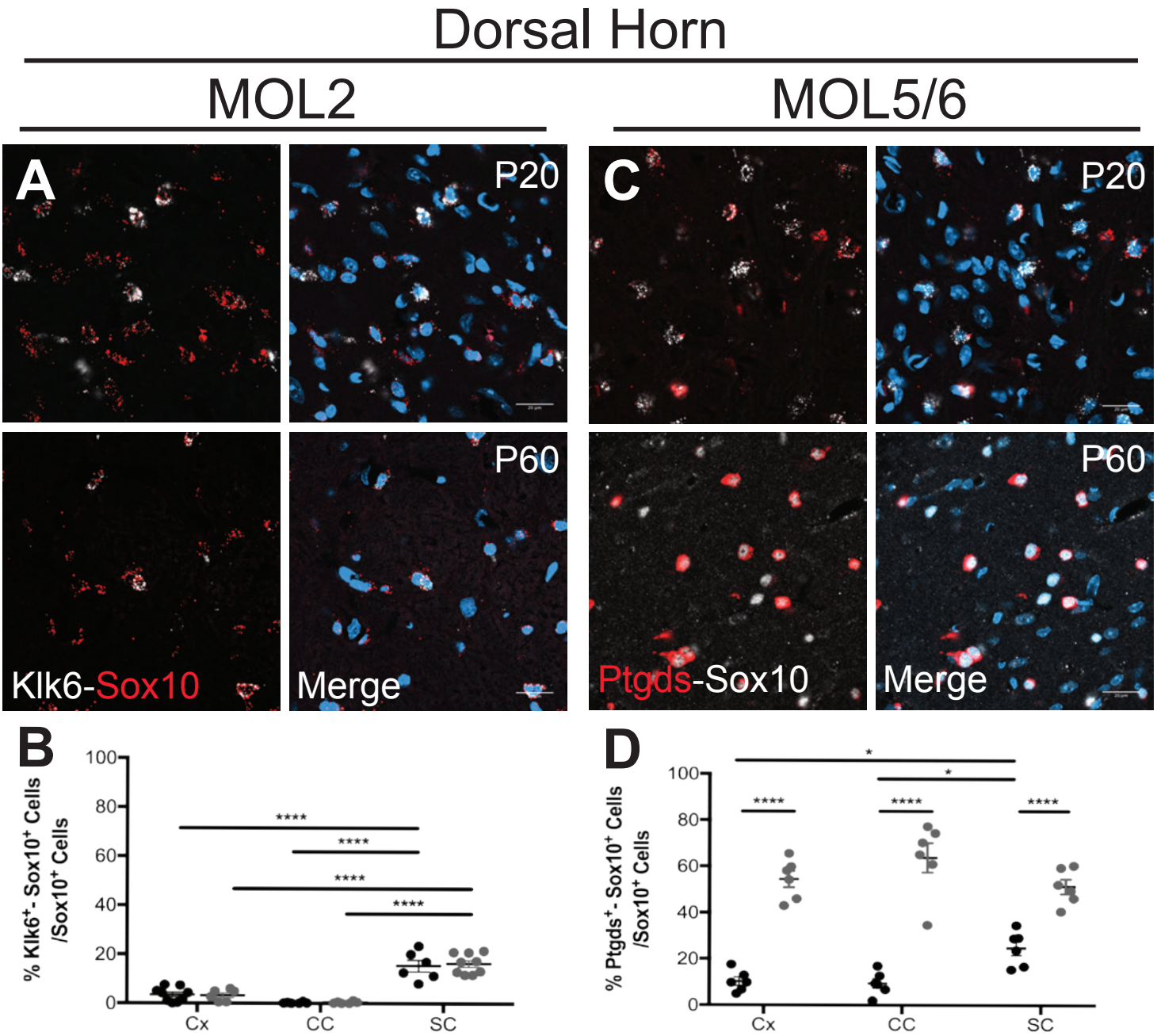

Floriddia et al, Fig. 2

Corpus Callosum

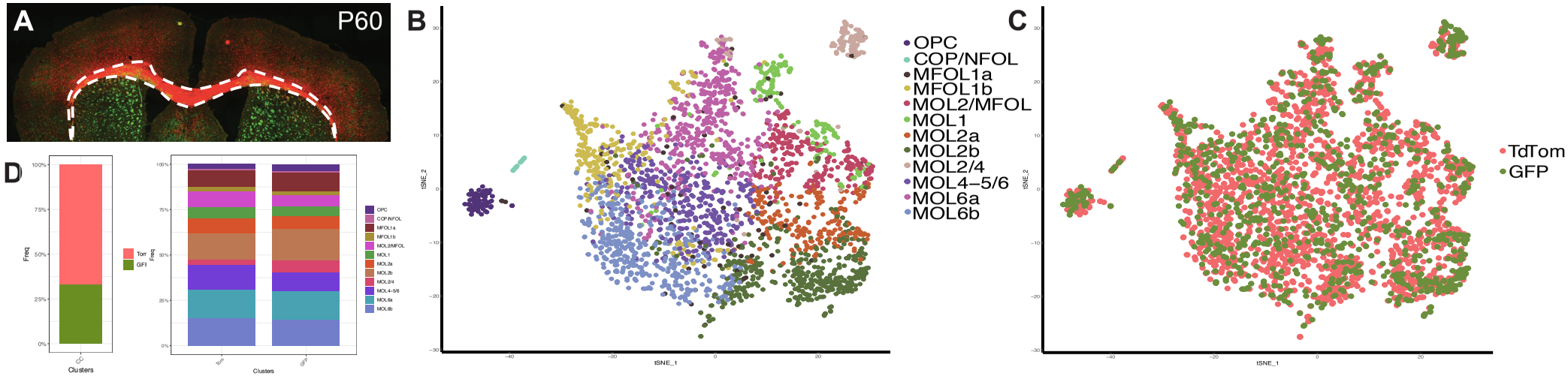

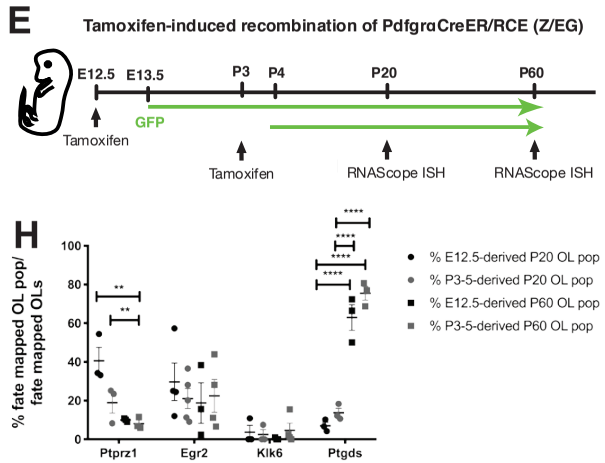

Lineage tracing of MOL5/6

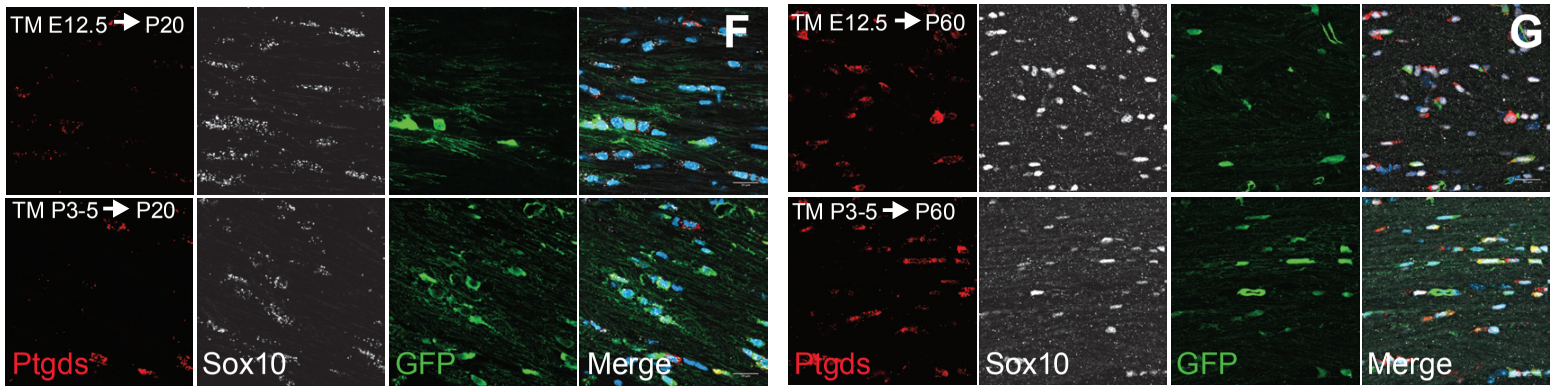

Floriddia et al, Fig. 3

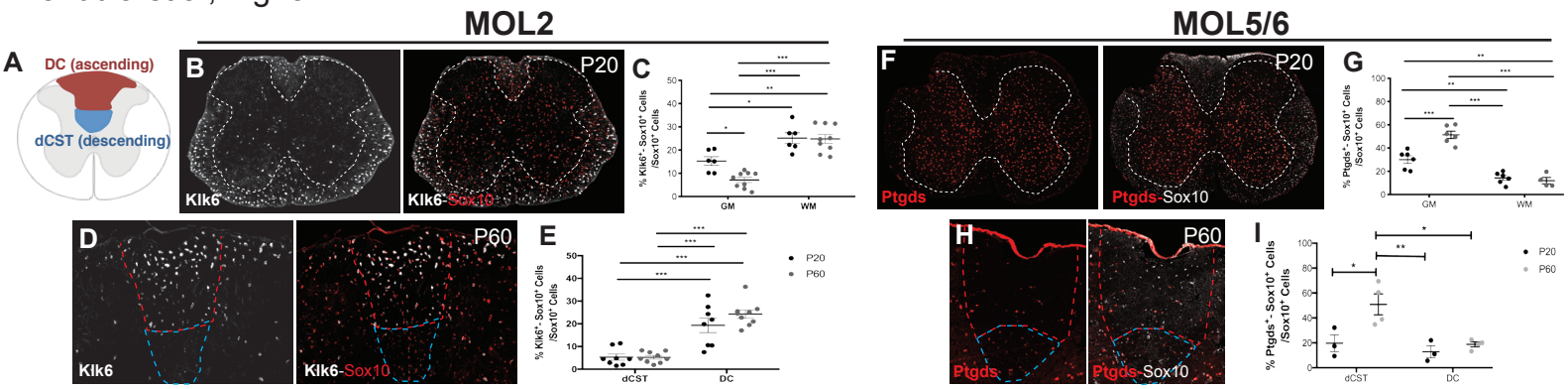
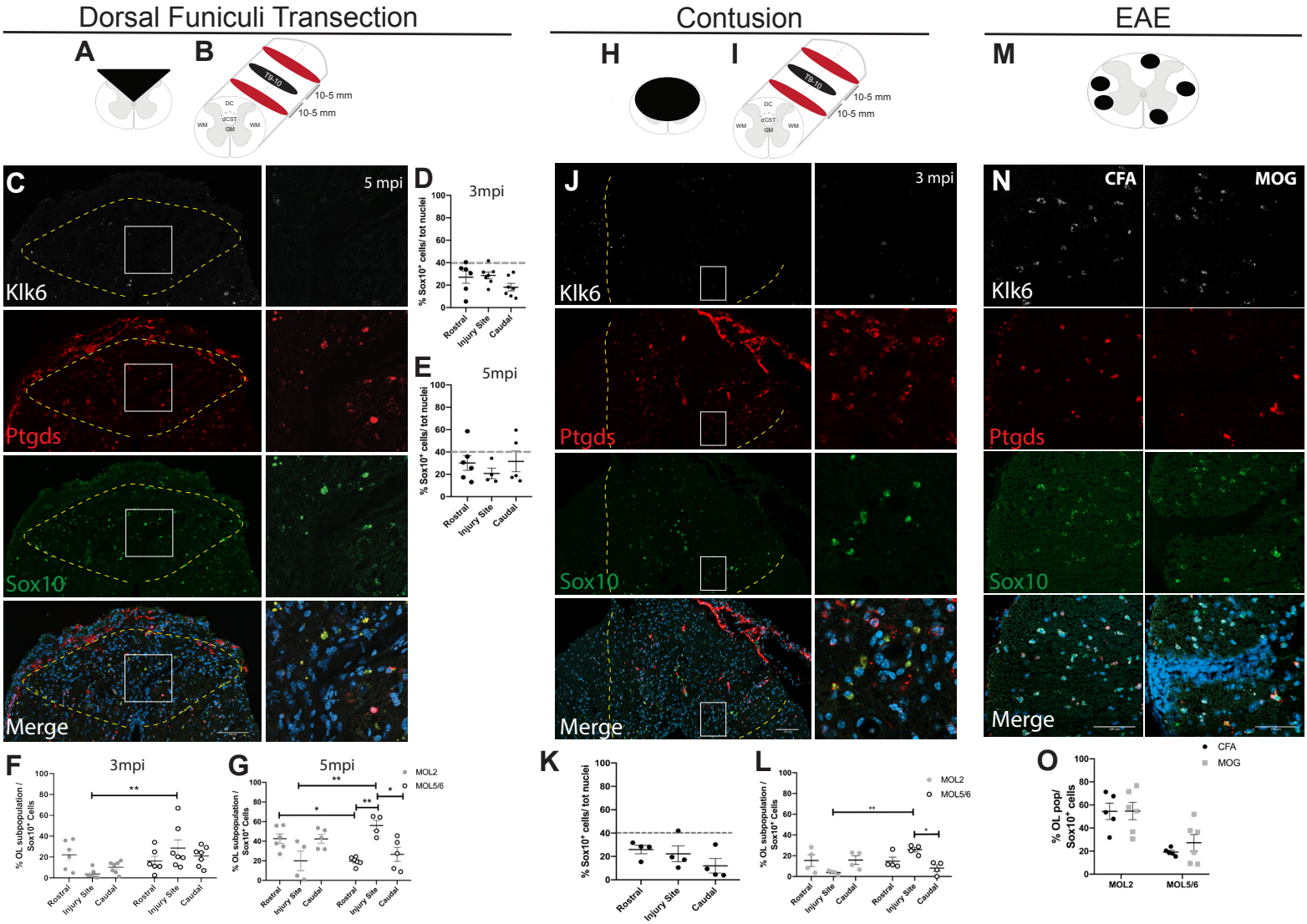
Floriddia et al., Fig. 4